Coherent phonons scattering by interstitial impurities in a quantum wire

Mohammed-Saïd Rabia

Coherent phonons scattering by interstitial impurities in a quantum wire

M.-S. Rabia

Université Mouloud Mammeri, Laboratoire de Mécanique des Structures et, Energétique,
15000 Tizi-Ouzou, Algeria
m2msr@yahoo.fr

Using the matching method formalism, this work presents the transmission and reflection coefficients of coherent phonons which propagate through a 1D quantum waveguide perturbed by the presence of reticular defects as interstitial impurities. Our waveguide model consists of two infinite atomic chains. The implied interactions refer only to the bonding strengths between nearest and next nearest close neighbours. .Numerical results show that the transmission spectra exhibit Fano-like resonance features which result from degeneracy of localized-impurity states and propagating continuum modes. In addition, the scattering by multiple impurities induces interferences between diffused and reflected waves in the defect region giving birth to Fabry-Pérot oscillations. This interference phenomenon could provide an interesting alternative to investigate structural properties of materials. The results could be also useful for the design of phonon devices.

1 Introduction

The survey of scattering and localization phenomena in the disordered mesoscopic systems interested the researchers at all times [1-3] because of the numerous applications found in classic metallurgy, in electrochemistry, in catalysis and in electronics.

Our present knowledge of the related phenomena has been given by the work of Landauer [4], in which the studied sample is represented by a set of scatterers (reticular defects) inserted in bulk or on surface of crystalline structure. He showed that the conductance of a quantum wire is bound directly to the scattering properties of such system, considered as a waveguide perturbed by defects. His approach has stimulated many researchers [5-10] to look for the effects of quantum coherence, most of the time by numerical methods, in dc transport particularly. Actually these phenomena are of renewed interest owing to advances in nanotechnologies, the basic motivation being to understand the limitations that reticular disorder may have on mechanical and vibrational properties of crystalline materials.

In the present work, we study the phonon's scattering by an interstitial impurity localized in an infinite double atomic chain. We analyze the behaviour of a plan wave which propagates throughout this crystal which is assimilated to a quasi-planar crystallographic waveguide. We concentrate in calculating the reflected and transmitted parts of the incidental wave, the phononic conductance as well as the displacements of the irreducible atoms composing the perturbed region. We are also interested by the determination of the localized induced impurity states especially important for transmission spectra interpretation. Different defect configurations are considered. The mathematical treatment of the problem resorts to the matching method [7,11] in the harmonic approximation framework [12-14] while using scattering boundary conditions.

2 Structural model

The considered model consists in two linear parallel periodic chains of masses, assimilated to a quasi-one-dimensional planar waveguide in which are incorporated interstitial impurities. The parallel chains are composed of specific masses aligned along the direction of propagation (x axis). The situation is depicted in Figure 1. Each mass is linked to its nearest and next nearest neighbours by harmonic springs of stiffness constants k_1 and k_2. The additional constants as K_{lv}, k_l and k_v, are represented on the figure. To simplify, the distances between adjacent masses are considered equal in the two Cartesian directions x and y of the plan. Also, to take account of the modification of the bonding strength field in the perturbed region (grey area M), we introduce a proportionality factor λ which indicates the ratio of the different force constants between the defect zone masses and those of the perfect lattice areas G (left) and D (right-hand side) located in sites separated by equivalent distances.

3 Matching method principle

Initiated by Feuchtwang in the sixties then revisited by Szeftel and *al.* in the eighties, the matching method returns account in a satisfactory way for the phonons dispersion curves [7-9] and for surface resonances. It gives also a more general definition of the resonance concept and allows a more transparent analysis of the displacements behaviour in the vicinity of the Van Hove singularities [15]. However, its execution requires the crystal subdivision in three distinct regions having all the same periodicity along the surface. The procedure was described in details in references [8]. We will just present the necessary stages to the comprehension of the results analysis.

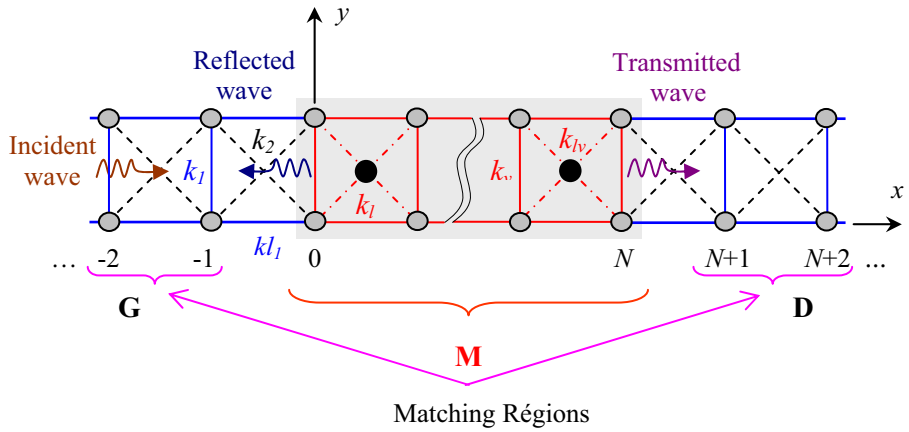

Figure 1: Schematic representation of a planar quasi-1D waveguide made up of two linear infinite chains perturbed by interstitial defects. The grey area M indicates defect region, G and D two semi infinite perfect waveguides.

3.1 Perfect lattice dynamics

For an atom occupying the site (l) and vibrating at the frequency ω, the equations of motion can be written, using the harmonic approximation framework [14], in the following form:

$$\omega^2 m(l)\, u_\alpha\left(l,\omega^2\right) = -\sum_{l'\neq l}\sum_{\beta} k(l,l')\frac{r_\alpha r_\beta}{d^2}\left[u_\beta\left(l,\omega^2\right)-u_\beta\left(l',\omega^2\right)\right] \quad (1)$$

where α and β represent the x, y directions of the plan; $m(l)=m$ indicates the atom mass located at site l; r_α is the component of the relative position vector between sites l and l', d the distance separating them and $k(l,l')$ the bonding strength constant between the two atomic sites.

Taking into account the problem symmetry and applying the scattering boundary conditions for which we get plan wave solutions, the perfect lattice atom equation of motion (1) rewrites itself in following matrix system:

$$\left[\Omega^2 I - D(Z,r_2)\right]\left|\vec{u}\right\rangle = \left|\vec{0}\right\rangle \quad (2)$$

where $\Omega=\sqrt{m\omega^2/k_1}$ is the dimensionless frequency, I the identity matrix, $D(Z,r_2)$ the (3×3) dynamical matrix of the perfect lattice and $|u\rangle$ the vector displacement. The r_2 parameter denotes the force constants ratio between nearest and next-nearest neighbours.

The scattering problem in presence of defects imposes the knowledge of both propagating modes ($|Z|=1$) and evanescent ones ($|Z|<1$) of the perfect waveguide. In other words, for a given frequency, all solutions are necessary even those whose module is lower than unity. These solutions can be obtained by increasing the eigenvectors basis:

$$\vec{v}_\beta(l) = -\frac{1}{Z}\vec{u}_\alpha(l)\,; \quad \beta = 5,\cdots,8\,. \quad (3)$$

We then rewrite equation (4) in the Z eigenvalue problem form,

$$A(\omega)\vec{W} = Z\,B\,\vec{W} \quad \text{with} \quad \vec{W}=\begin{pmatrix} u_\alpha(l) \\ v_\beta(l)\end{pmatrix}, \quad (4)$$

where A and B are (4×4) matrices coming from the basis change. Let us note that the dimension of this generalized eigenvalue problem is twice as large as the original problem.

3.2 Coherent phonons scattering at defects

Since the perfect waveguides do not couple between different eigenmodes, we can treat the scattering problem for each vibratory eigenmode separately. Generalization to every combination of these modes does not pose a particular problem. For an incoming wave from the left of Figure 1 in the eigenmode $\bar{\nu}$,

$$\vec{V}^{\,i}_{in} = (Z_{\bar{\nu}})^i\,\vec{u}_{\bar{\nu}}\,, \quad i\le -1 \quad (5)$$

where $Z_{\bar{\nu}}$ is the attenuation factor of the entering mode, $\vec{u}_{\bar{\nu}}$ its eigenvector; the superscript $i\,(\le -1)$ indicates the site occupied by the atom with respect to the direction of propagation.

The resulting scattered waves are composed of a reflected and transmitted parts, which can be expressed as a superposition of the eigenmodes of the perfect waveguide at the same frequency, i.e.,

$$\vec{u}^{\,i}_r = \sum_\nu r_{\nu\bar{\nu}}\cdot\left[\frac{1}{Z_\nu}\right]^i.\vec{u}_\nu\left(\frac{1}{Z_\nu}\right), \quad i\le -1 \quad (6)$$

$$\vec{u}^{\,i}_t = \sum_\nu t_{\nu\bar{\nu}}\cdot\left[Z_\nu\right]^i.\vec{u}_\nu(Z_\nu), \quad i\ge 2 \quad (7)$$

where $r_{\nu\bar{\nu}}$ and $t_{\nu\bar{\nu}}$ indicates the reflection and transmission coefficients normalized beforehand by group

velocities (slopes of the dispersion curves in Figure 2) of the plan wave, set equal to zero for the evanescent modes. The evanescent modes are needed for a complete description of scattering in presence of defect, although they do not contribute at all to the energy transport.

With the definitions (6) and (7), we can rewrite the dynamical equations for the perturbed double chain. Since there are perfect waveguides in regions G and D, we only need to solve Eqs. (1) for the masses inside the perturbed zone M and in the boundary columns (-1) and (2), which are matched to the rest of the perfect waveguide by Eqs. (6) and (7). Isolating the inhomogeneous terms describing the incidental wave, we obtain an inhomogeneous system of linear equations

$$\left[D_f(\Omega, r_2, \lambda, Z)\right]\left[R\right]\vec{X} = -\left[D_f(\Omega, r_2, Z)\right]\vec{V}_{in} \qquad (8)$$

where $D_f(\Omega, r_2, \lambda, Z)$ indicates the dynamical defect matrix, $\vec{X}$ the vector gathering all the problem unknowns, $\vec{V}_{in}$ the incidental vector and R the matching matrix.

As example, for an isolated defect we obtain a dynamical matrix $\tilde{D}\left[18\times 26\right]$; from where a matching matrix $R\left[26\times 18\right]$ is deduced. Then the vector $\vec{X}$ will be composed of eighteen unknowns including the ten displacements $u_\alpha(l)$ of the irreducible atoms, the four transmission coefficients and four reflection ones.

4 Numerical results and discussion

4.1 2D and 3D dispersion curves

For $Z = e^{iqa}$, the resolution of the equation (2) determines the eigenfrequencies Ω_ν as well as the corresponding eigenvector $\vec{u}_\nu$. The propagating modes correspond to the solutions $|Z| = 1$. They are usually given in terms of q, with q running over the first Brillouin zone $\left[-\frac{\pi}{a} \quad \frac{\pi}{a}\right]$. In the case of the double chain, we obtain two acoustic modes with $\Omega \to 0$ when $q \to 0$. The two remaining modes are optical with $\Omega \neq 0$ for any q. Figure 2 shows the curves of dispersion $\Omega(q)$ for $k_1 = 1$, $r_2 = 0.5$ and $m = 1$. Contrary to the electronic case where the curves are parallel sinusoids, we do not have here any hope to find a usable analytical expression. It will thus be necessary to resort to purely numerical methods to integrate this dispersion relation in the general problem in presence of defect.

The analysis of the eigenvectors indicates that the waveguide eigenmodes are either symmetric or antisymmetric relatively to the central axis confused with the propagation direction. The results show that there is one acoustic and one optic mode for each symmetry. Moreover, the anticrossing behaviour between the symmetric acoustic and optic modes observed in Figure 2 is due to the fact that the dispersion curves belonging to the same symmetry interact and therefore do not cross. Note further that the antisymmetric transverse acoustic mode has q^2 dispersion for $q \to 0$ [16]. This behaviour is a consequence of the finite extension of the waveguide in y direction.

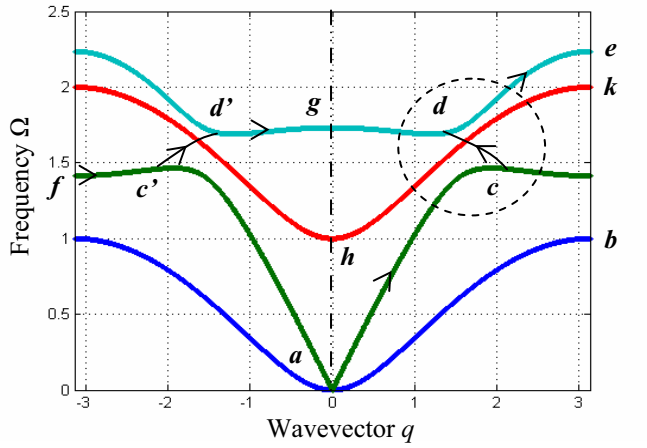

Figure 2: Phonons dispersion branches for propagating modes for a quasi planar waveguide represented by two infinite atomic chains with real q running over the first Brillouin zone for $k_1 = 1$, $k_2 = 0.5$ and $m = 1$.

On Figure 3 are represented the functional behaviours of the four vibrating modes characterizing the double chain. They are obtained by resolving Eq. (4). Common special points are knowingly considered in the two representations $\Omega(q)$ and $\Omega(Z)$ to facilitate the comparison between 2D dispersion curves (Figure 2) and the 3D curves (Figure 3). The projection of the curves on the complex plan shows that the propagating solutions follow the circles of unit radius, equal to the phase factor module; whereas the evanescent solutions correspond to the curves contained inside the unit circle.

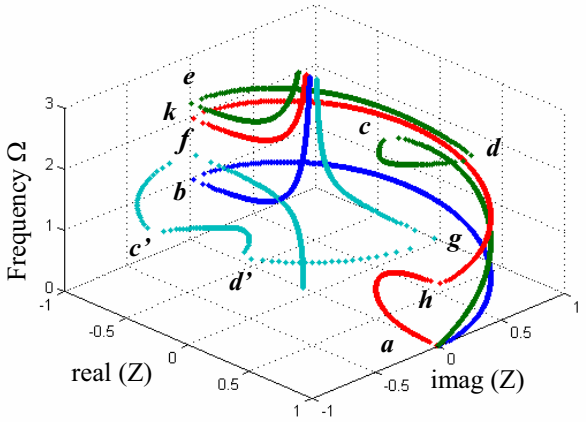

Figure 3: Functional behaviours $\Omega(Z)$ of the vibrational modes characterising the double atomic chain. Unit circles correspond to propagating modes (dispersion curves $\Omega(q)$, Figure 2) whereas the evanescent modes are represented by the parts inside the unit circles.

The two antisymmetric modes are degenerated at the point a ($Z = 1, \Omega = 0$). The acoustic mode is propagated up to the point f where $\Omega = \Omega_f$ and $Z = -1$. It becomes evanescent for larger frequencies.

Starting from point *a*, the other solution is immediately evanescent at the low frequencies then follows the optical branch of discrepancy between points $h(Z=1)$ and $k(Z=-1)$ to become evanescent again. For still higher frequencies $\Omega > \Omega_k$, the two solutions follow the real negative Z axis and remain evanescent when $|Z| \to 0$ and $\Omega \to \infty$.

For the symmetric modes, the functional behaviour is somewhat more complicated. This is essentially due to the anticrossing phenomenon of the propagating acoustic and optic modes of the same symmetry, which constrained phonons to take evanescent paths to jump from a propagating branch to the other in the interacting zone, surrounded by a dashed circle in Figure 2 [8,9]. The solution starting at point *a* follows the propagating acoustical mode up to point *c*, which corresponds to the maximum frequency in this branch. It then joins the minimum of the optical branch by taking an evanescent path with $|Z| \neq 1$. From point *d* to *e*, it continues on the propagating optical branch, before becoming again evanescent with real negative *Z*. The second solution is evanescent for $\Omega = 0$, starting with a real negative value of *Z*. For increasing frequencies, it follows the negative *Z* axis to reach point *f* in the propagating optical branch, continues on this propagating branch up to its maximum frequency at point *c'* and then joins point *d'* on the propagating optical branch via an evanescent path. It coincides with the propagating optical branch between points *d'* and *g* and then becomes evanescent with real positive *Z*. For higher frequencies, both solutions remain evanescent with $|Z| \to 0$ when $\Omega \to \infty$

4.2 Single impurity scatterer

Phonons scattered by impurity are analyzed relatively to an incidental wave coming from the left of Figure 1, with unit amplitude and a zero phase on the border atom (-1) located just at the beginning of the defect region *M*. The numerical results for the transmission and reflection coefficients in terms of the incident phonon frequency are consigned in Figure 4 in the case of light impurity mass $m' = 0.5\,m$.

We notice that the presence of the interstitial defect leads to a general decrease of the probability amplitude. As expected, the influence of the defect is relatively small in the acoustical regime because of the low implied frequencies. For $\Omega \to 0$, we get $T_\nu \to 1$; the subscript ν (=1 to 4) refers to the dispersion curves of Figure 2, where the modes are numbered from bottom to top. Moreover, the transmission spectra are marked by pronounced typical Fano-like resonances (indicated by arrows in Figures 4). These asymmetric resonances can be attributed to the presence of impurity-induced resonant states, whose frequency depends on the value of the bonding forces in region *M*. Consequently, these resonances take place at low frequencies for heavy defects and inversely for the light ones. These findings are in agreement with those of Tekman and Bagwell [2], who used a two mode-mode approximation.

Lastly the well known theoretical relation translating the conservation of energy principle,

$$\left(|R_\nu| + |T_\nu| \right) = 1 \qquad (9)$$

is fortunately satisfied and always checked for each frequency. Besides, this condition constitutes an effective control method of the results.

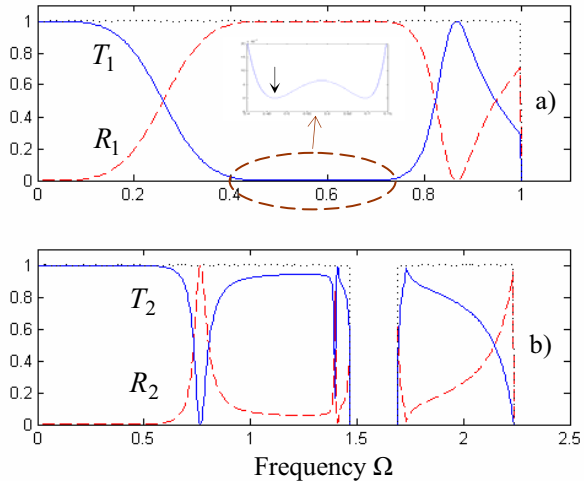

Figure 4: Transmission and reflection coefficients as a function of the phonon frequency for an isolated interstitial defect in a) acoustic mode 1 and b) optical mode 2 in the case of light impurity mass ($m' = 0.5\,m$). The arrows indicate the Fano-like resonance peaks; the dotted curve shows the good complementarity between the two coefficients.

The results of the conductance $\Lambda(\Omega)$ are shown on Figure 5. In addition to the curves of conductance relating to each impurity mass considered previously, we also represented that of the perfect lattice (dash-dawned curve).

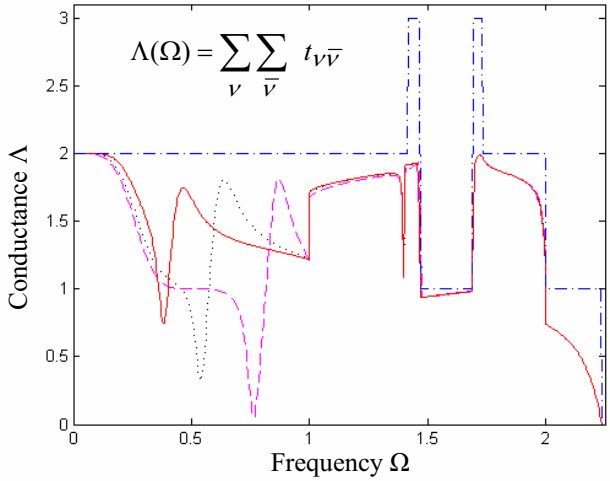

Figure 5: The total transmission probability vs phonon frequency for impurity masses $m' = 0.5\,m$ (dashed line), $m' = m$ (dotted line) and $m' = 2\,m$ (full line) in the case of a single impurity scatterer. The dashed histogram represents the total hypothetical phonon transmission capacity of the system.

In this case, the entering wave is totally transmitted in each propagating mode. The conductance of the system becomes then more important where the modes overlap. For this reason, its value reaches more than unity in the se concerned frequencies range.

Otherwise the conductance spectrum is much more affected in the case of light impurity mass (dashed curve). In addition to resonance, this influence is translated by a less amplitude compared to for bigger masses at weak frequencies.

4.3 Extended defect

The increase of the defect region width doesn't bring anything of qualitatively new in relation to the case of the single impurity. The addition of impurities results solely in the increase of the size of the linear system (6), but the matrix $\tilde{D}$ keeps its structure. The supplementary blocks have the same shape as those characterizing a single defect. We have limited our study to only ten interstitial impurities which already generates a (72×80) defect matrix dimension. The effects described previously in the case of isolated step appear, but they are even more difficult to isolate because of the biggest number of peak-dip structures near in frequencies. It is why we are not going to study in details these regions. On the other hand, we will limit ourselves to present a more global change of the transmission curves, provoked by the Fabry-Pérot oscillations issued from interferences between the multiple scatterings of propagating states in the perturbed region.

The phonon scatterings, considered for an extended defect composed of several interstitial impurities, are presented in Figures 6 and 7 for light mass impurity ($m'=0.5\,m$) and a heavy one ($m'=2\,m$). It can be seen that the transmission curves structure became richer of several peaks. We observe also a drastic dependence of Fabry-Pérot oscillations with the number N of impurities. However, the number of main dips remained the same corresponding to the total number of lattice parameter a contained in the width of the perturbed region.

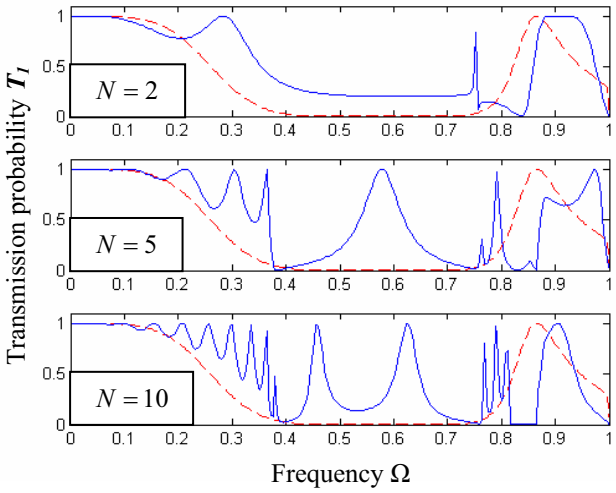

Figure 6: Transmission coefficient as a function of the phonon frequency for an extended defect composed of N defects of light impurity mass $m'=0.5\,m$. The dotted curve refers to an isolated scatterer having the same mass.

The fact that their number seems to be lower on the figures is simply related to a resolution problem in the implied frequency range. Same results are observed by V. Pouthier and *al*. [17] on the transmittance spectrum of a nanowire containing a set of linear clusters separated by different spacing. Otherwise, the upper level of the Fabry Pérot oscillation can merge with the Fano-resonance peak. It should be noted that on average the global shape of the transmission curves is quite similar to that obtained in the case of an isolated impurity (in dashed line on the figures).

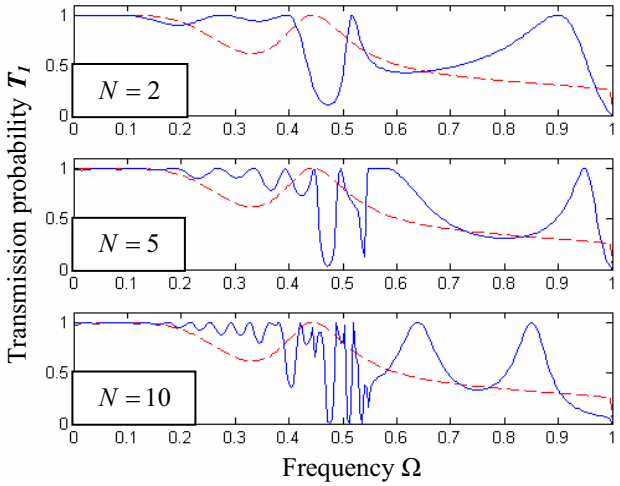

Figure 7: As in Figure 6 for a heavy impurity mass ($m'=2\,m$).

The transmission curves are turned into a number of peak-dip structures, the reason is that the modes will interfere with each other due to the multiple reflections of the phonon waves in the perturbed region. In general, the multiple interferences in the perturbed waveguide imply the more complex transmission spectra. These interferences between multiply scattered waves result in Fabry–Pérot oscillations of increasing amplitudes with the frequency and whose number depends intimately of the number N of impurities. Similar results are obtained in the study of adatomic defects [8,9,16-19] and substitutional defect columns [8] in the perturbed double quantum chain. Defects are separated by different spacing in both configurations

5 Conclusion

In this work, we have analyzed the behaviour of propagating elastic waves through a quantum waveguide perturbed by interstitial impurities. Our calculation resorts to the matching procedure based on the Landauer-Büttiker approach. The scattering is considered for isolated and extended impurities defects. In both configurations, strong asymmetrical resonances are observed in the transmission spectra; these structures are allotted to the coupling discrete continuum-states induced by the defect region *M*. The resonance peaks and their number are determined also by the width of the perturbed region M, i.e. the number N of impurities. Moreover, the transmission spectrum is also characterized by other oscillations of Fabry-Pérot type due to the interferences between transmitted ant reflected waves in the perturbed region. Their number depends closely of the defect region width.

The transmission spectra can thus be used for identifying defects of specific structures and then being

used for their characterization. The interference effects are of interest for improvements in the design of transducers and noise control [20] whereas Fano-type resonances are commonly used to build filters [21]. The results could be also useful for the design of phonon devices.

References

[1] B. Kramer, *Quantum Coherence in Mesoscopic Systems*, (plenum, New York, 1991).

[2] E. Tekman and P. F. Bagwell, *Phys. Rev*., B48, 18 299 (1993).

[3] Kosevich Yu.A. 1997 Prog. Surf. Sci. vol 55, 1.

[4] R. Landauer, *Z. Phys.* B 68, 217, 8099 (1987) ; *J. Phys. Condens. Matter*, 1, 8099 (1989).

[5] M. Büttiker, *Phys. Rev. Lett*., 57, 1761 (1986).

[6] Syrkin E.S., Minaev P.A, Shkorbatov A.G. and Feher A 2005 Microelec. Eng. vol. 81 p 503.

[7] J. Szeftel and A. Khater, *J. Phys C*, 20,4725 (1987).

[8] A. Fellay, F. Gagel, K. Maschke, A. Virlouvet and A. Khater, *Phys.Rev*, B 55, 1707 (1997).

[9] M. S. Rabia, *J. Mol. Struc-Theochem*, 777, 131-138 (2006).

[10] A. Khater, N. Auby and D. Kechrakos, *J. Phys. Condens. Matter*, 4, 3743-3752 (1992).

[11] T. E. Feuchtwang, *Phys. Rev.,* **155**, 731 (1967).

[12] R. F. Wallis, *Surf. Sci.* **2**, 146 (1964).

[13] A. A. Maradudin, and J. Melangailis, *Phys. Rev*. A 133, 1118 (1964).

[14] A. A. Maradudin, E. W. Montroll, G. H. Weiss and Ipatova, *Theory of lattice Dynamics in the Harmonic Approximation,* Academic Press New York and London (1971).

[15] L. Van Hove, *Phys. Rev.* **89**, 1189 (1953).

[16] M. S. Rabia, H. Aouchiche and O. Lamrous, *Eur. Phys. J. – A. P.* 23, 95-102 (2003).

[17] V. Pouthier and C. Girardet, *Phys. Rev.* B 66*,* 115322 (2002).

[18] W. Kress, F. W. De Wette (Eds), *Surface Phonons*, (Springer-Verlag, Berlin, 1991).

[19] M. S. Rabia, *J. Physica E 42,* 1307-1318 (2010).

[20] M. Guglielmi, F. Montauti, L. Pellegrini, and P. Arcioni, *IEEE Trans. Microwave Theory Technol,* **43**, 1991 (1995).

[21] M. S. Kushwaha, A. Akjouj, B. Djafari-Rouhani, L. Dobrzynski, J.O. Vasseur, *Solid State Commun.* 106, 659 (1998).